Journal of Materials Chemistry A

Accepted Manuscript

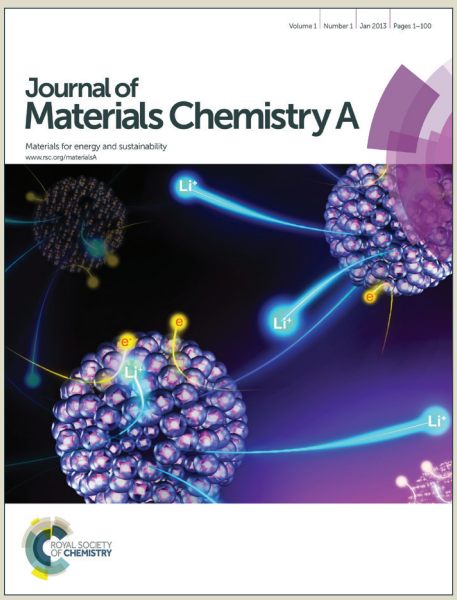

ROYAL SOCIETY OF CHEMISTRY

www.rsc.org/materialsA

Nanostructured ZnO/Sepiolite Monolithic Sorbents for H_2S Removal†

Raquel Portela,*γa Fernando Rubio-Marcos,γb Pilar Leret,c José F. Fernández,b Miguel A. Bañaresa and Pedro Ávila.a

a Instituto de Catálisis y Petroleoquímica (ICP), CSIC. Marie Curie 2, L10, E-28049 Madrid, Spain. raquel.portela@csic.es

b Electroceramic Department, Instituto de Cerámica y Vidrio (ICV), CSIC. Kelsen 5, E-28049 Madrid, Spain.

c Advanced Dispersed Particles S.L. Research & Development Division. Oro 45, nave 14, E-28770, Colmenar Viejo, Madrid, Spain

γ **Author Contributions:** R. Portela and F. Rubio-Marcos contributed equally.

† **Supporting information available**

Keywords: Hydrogen sulfide; sulfur dioxide; ZnO; clay; monolith.

Abstract

ZnO presents favorable thermodynamics, equilibrium constant and stability for H_2S chemisorption and sepiolite has excellent sorptive and rheological properties to be employed as support. Four conformed ZnO/sepiolite composites are prepared, two by impregnation in zinc nitrate solution -one using activated carbon as dispersing and pore generating agent- and two by dry mixing of the clay with dispersed or hierarchically assembled ZnO nanoparticles. The extrudates obtained with a mixture of sepiolite and nanodispersed ZnO particles are the most active for H_2S chemisorption in temperature-programmed tests performed in inert atmosphere, which can be correlated to the higher and homogeneous ZnO dispersion. ZnO sulfidation is reversible in the presence of O_2. Thus, the activity can be regenerated, and these materials act as catalysts for H_2S to SO_2 oxidation in air.

1. Introduction

Hydrogen sulfide must be removed from gaseous streams emitted to the atmosphere, in order to meet environmental and safety regulations, and also from streams that are further used in industrial processes, to prevent downstream catalyst poisoning and corrosion. Many technologies are available for H_2S elimination; oil and natural gas refining industry typically uses the Claus process (large, concentrated gas streams), whereas H_2S sorption is a common solution for trace amounts. H_2S sorbents are widely used due to their efficiency and reliability; zeolites,[1] activated carbon,[2] clays,[3] and metal oxides[4] such as CaO, Fe_2O_3, MnO_2, ZnO, etc. have been studied in desulfurizing processes. H_2S removal mechanism may involve physical adsorption onto the solid surface or the liquid water film formed thereon, dissociation, reaction with metal oxides to form sulfides, with alkaline species to give neutralization products, or with surface oxygen species to give redox reaction products such as elemental sulfur or sulfate. Among metal oxides, Zn-based sorbents are very attractive for H_2S removal because of the favorable thermodynamics and the high equilibrium constant for the non-catalytic sulfidation reaction, and also due to the thermal stability of the sorbents and their sulfides.[5, 6] Various commercial products use zinc oxide and operate in the 200-400 °C range; the maximum sulfur loading on these products is typically 300-400 mg S/g sorbent.[7] It is believed that this gas–solid reaction is controlled at low temperature by either diffusion of HS^- into the pores (H_2S is known to dissociatively adsorb as HS^- and H^+ on ZnO surface) to react with the oxide or by lattice diffusion of generated water and fresh oxide that migrates to replenish the sulfided surface.[8] High temperatures may lead to ZnO volatilization or thermal sintering, reducing the activity.[9] Moreover, phenomena like reduction of the oxide must be avoided. Aforementioned sintering or volatilization risks also apply to the process of regeneration of the oxide with oxygen to generate highly concentrated SO_2 and recover the sorption capacity. Additionally, stable undesired $ZnSO_4$ may be produced when the regeneration is carried out at low temperatures or with high content of oxygen;[10] meanwhile, from an economic point of view, in order to obtain SO_2 concentrations suitable for H_2SO_4 production, the oxygen molar fraction in the feed gas should be higher than 10%.

Multi-component sorbents may present synergetic effects for H_2S elimination. Fe, Co, Ni, Cu, Al, Ti, Mn or Ce are typical promoters of Zn-based sorbents.[11] These may help achieving high sulfidation yields even at low temperatures.[4] On the other hand, supporting

the oxides may minimize volatilization, reduction and sintering problems during sulfidation and regeneration,[10, 12] increase the surface area and porosity, and disperse the ZnO particles. Besides, with appropriate supports conformed materials may be obtained by extrusion.[13] In this mainly unexplored line, sepiolite seems very interesting as support for ZnO-based H_2S sorbents. Up to now, ZnO/sepiolite mixed materials have only been prepared in powdered form by sol–gel method, being successfully tested for the photocatalytic degradation of a dye.[14] Sepiolite is a natural hydrated magnesium silicate fibrous clay with inter- and intra-particle porosity and chemical composition $Si_{12}Mg_8O_{30}(OH)_4(H_2O)_4 \cdot 8H_2O$, which possesses excellent sorptive, rheological and catalytic properties for multiple applications.[15, 16] It has been employed as support and binder for composites with metal oxides, especially TiO_2, for catalysis [17] and photocatalysis;[18, 19] the combination of photocatalytic and adsorptive properties in TiO_2/sepiolite composites has given interesting results for H_2S removal.[19, 20] Additionally, sepiolite may catalyze the Claus reaction.[21, 22]

The synthesis is a key component in the economic and environmental value of synthetic materials. In industrial practice, supported metal and metal oxides constitute the most important group of heterogeneous catalysts and thus their synthesis is of greatest scientific and manufacturing importance. Certainly, the most common synthesis routes comprise the impregnation of a preexisting support with a solution of a metal salt, and differ in terms of solvent (polar or nonpolar), metal salt choice, and post-impregnation treatments.[23-25] The dispersed active phase (i.e., the metal oxide or the metal in the reduced state) is usually obtained after a thermal treatment. The fundamental phenomena underlying impregnation and drying steps are extremely complex though the practical execution is apparently simple. Typically, metal precursor and support interactions are limited, thereby permitting the redistribution of the active phase over the support body during drying. Finally, a reagglomeration of the active phase occurs frequently due to the evaporation of the solvent taking place on the outer surface of the support particles. Alternatively, the use of dry mixing procedures has been demonstrated as an efficient route to tailor catalytic performance.[26, 27]

The scope of this work is to obtain conformed solids with high surface area and porosity containing a good active phase for H_2S sorption, ZnO, preserving the nanodispersion and the sulfidation capacity. Nanostructured composite materials containing sepiolite and disperse ZnO nanoparticles have been prepared by impregnation and dry mixing methods

and conformed as monoliths by extrusion. Their activity for H_2S chemisorption has been evaluated.

2. Experimental Section

2.1. Synthesis

Four different conformed composites were prepared with α-sepiolite (Pansil 100, Tolsa) as support, having a composition of 20/80 wt./wt. ZnO/sepiolite. This composition ratio was choosen according to the surface area of ZnO and sepiolite, ~20-30 and ~120-130 m^2/g respectively, in order to maximize the appearance of ZnO/sepiolite interphases. Two samples were prepared by wet impregnation in excess water, using a solution of a zinc salt as precursor of the oxide ($Zn(NO_3)_2.6H_2O$, Sigma Aldrich), and the other two by dry mixing of the sepiolite with ZnO nanoparticles. The composition ratio was kept constant in the different composites as a way to evaluate the effect of the ZnO nanoparticles dispersion in the cataltytic activity.

Impregnation procedures (ZnO-I and ZnO-ICP series):) An aqueous solution with 8.3 g of the salt was impregnated onto 4.7 g of sepiolite by two different methods: either directly onto the sepiolite powder (samples hereafter named as ZnO-I), or, following the previously reported impregnated carbon procedure,[28] first onto 4.7 g of activated carbon (Pulsorb FG5), to which the sepiolite was subsequently added(samples henceforth referred to as ZnO-ICP).

Dry mixing procedures (ZnO-N and ZnO-NH series): The sepiolite powder was manually mixed with the metal oxide nanoparticles. Two different types of nanoparticles were used. In the case of the samples named ZnO-N, commercially available nanosized zinc oxide was employed (99.99%, SkySpring Nanomaterials Inc.). The morphology of this material is characterized by small spherical particles of 15-30 nm, which are forming globular agglomerates, see Supporting Information Figure S1(a). On the other hand, the catalyst named ZnO-NH was prepared using hierarchically organized nanoparticles of zinc oxide that were synthesized by a solvothermal method previously reported by Jianxing Shi *et al*.[29] The morphology of the hierarchical material employed is characterized by ZnO nanoparticles of ~20-25 nm aggregated to form uniform spheres of ~ 400 nm, as it is observed in the FE-SEM image of Figure S1(b).

In order to make extrudates, the necessary amount of water was added to all the dry-mixed ZnO/sepiolite powders and wet-impregnated supports. The smples were manually kneaded for some minutes until adequate rheological properties were achieved, then the doughs were manually extruded with a syringe and cut in the shape of pellets (d=1.86 mm,

L=5 mm). Finally, for comparative reasons and to ensure the dehydration of the sepiolite and the complete removal of precursor remnants in the impregnated materials, all samples were dried at room temperature and heat treated at 500 ºC for 4 h in air.

2.2. Physico-chemical characterization

Thermal characterization: Simultaneous thermogravimetric and differential thermal analyses (TGA-DTA) of $Zn(NO_3)_2 \cdot 6H_2O$, which was used as ZnO precursor in the impregnation and impregnated carbon procedures, were carried out in a flowing air atmosphere using a NETZSCH STA 409/C analyzer. Around 50 mg of powder were placed in a Pt/Rh crucible and heated up to 600 ºC with a heating rate of 3 ºC/min.

TGA-DTA coupled with gas-phase Fourier transform infrared (FTIR) spectroscopy was used to characterize the uncalcined, calcined and used composites. The analysis was performed in a simultaneous thermal analizer (STA 6000) connected to a Frontier IR spectrometer equipped with a gas cell, both from PerkinElmer. Around 15 mg of powder were placed in alumina crucibles and submitted to a temperature ramp of 10 ºC/min up to 950 ºC in air flow atmosphere. IR spectra were collected from 650 to 4000 cm^{-1} at a resolution of 2 cm^{-1} with 2 accumulations.

Structural characterization: The phase identification was performed by X-ray diffractometry (XRD, X'Pert PRO Theta/2theta, PANalytical, The Netherlands) on powder obtained by milling the ZnO/sepiolite monoliths at room temperature. The patterns were recorded over the angular range 5–70° (2θ) with a step size of 0.0334° and a time per step of 100 seconds, using Cu Kα radiation (λ = 0.154056 nm) with working voltage and current of 40 kV and 100 mA, respectively.

Morphological and chemical characterization: The particle size and morphology of the powders were evaluated using a JEOL 2100F transmission electron microscope (TEM/HRTEM) operating at 200 KV and equipped with a field emission electron gun providing a point resolution of 0.19 nm. For TEM sample preparation, the particles were carefully suspended in ethanol. The suspension was dropped on a copper TEM grid with carbon film support. The particles were kept at the grid after evaporation of ethanol. The microscope is coupled with an INCA x-sight energy dispersive X-ray spectrometer (EDXS), from Oxford Instruments, used for chemical elemental analysis. Additional chemical

analyses were performed by inductively coupled plasma-optical emission spectroscopy (ICP-OES) in a PerkinElmer Optima 3300DV instrument.

Textural characterization: Specific surface area data were calculated from nitrogen adsorption/desorption isotherms obtained at −196 °C in an ASAP 2420 apparatus (Micromeritics), after application of the BET equation. Cumulated pore volume and pore size distribution data in the meso- and macro-pore range were determined in an AutoPore IV 9510 mercury intrusion/extrusion porosimeter (Micromeritics). Pore size was calculated using the Washburn equation for cylindrical pores: Pore diameter = -(4γ cosθ)/P, where γ=surface tension (484 mN m^{-1}), P=pressure, and θ=contact angle (141 º).

2.3. Catalytic activity tests

The activity for H_2S elimination was evaluated in a stainless steel tubular reactor (ϕ_{int} = 7.5 mm) filled to a height of 117 mm with 3 g of material (0.6 g ZnO). The gas flow rate was 1 $L \cdot min^{-1}$, corresponding to a GHSV of 11485 h^{-1} and a linear velocity of 0.37 $m \cdot s^{-1}$, and the concentration of H_2S was 450 ppm_v. The gas phase composition was analyzed with an online microGC (CP4900, Varian). After stabilization of the pollutant concentration in bypass, the gas flow was passed through the reactor at 50 ºC. When the adsorption equilibrium was reached the reactor was submitted to a heating ramp from 50 to 500 ºC at 1 ºC/min, and then maintained at this temperature until deactivation. Blank tests with SiC, as a reference inert material, and with pure sepiolite, as reference for the effect of the support, were performed in the same conditions.

3. Results and Discussion

3.1. Thermal behavior, physico-chemical properties and morphology of the ZnO/sepiolite systems

Thermal analysis methods are used to establish the conditions in which the precursor, $Zn(NO_3)_2 \cdot 6(H_2O)$, decomposes to ZnO. TGA and DTA curves in Figure S2 of the supporting information suggest three steps which occur during the progressive heating of the coordination compound. $Zn(NO_3)_2 \cdot 6(H_2O)$ exhibits two endothermic dehydration DTA peaks in the 25-260 ºC temperature range. The associated TGA weight losses correspond to the evolution of 4 and 2 water molecules, respectively. This behavior has been previously described for different transition metal precursors, which are based on $M(NO_3)_2 \cdot 6(H_2O)$ (M=metal).[30] The final strong endothermic effect, with maximum at 340

ºC, is due to ligands combustion with liberation of gaseous nitrogen oxide, and finally, the formation of ZnO by reaction with oxygen. These facts indicate that the thermal treatment should be performed at temperatures over 400 ºC. Based on these results, and on the temperature required to consolidate the anhydrous sepiolite structure[31] and to burn out the carbon of the ZnO-ICP sample, the heat treatment selected was 500 ºC for 4 h for all samples. Figure 1 elucidates the thermal decomposition process of ZnO-I (a) and ZnO-ICP (b) composites. DTA-TGA-FTIR data guarantee the complete decomposition of the $Zn(NO_3)_2 \cdot 6(H_2O)$ precursor and, in the case of the the imprenated carbon procedure, also of the activated carbon.

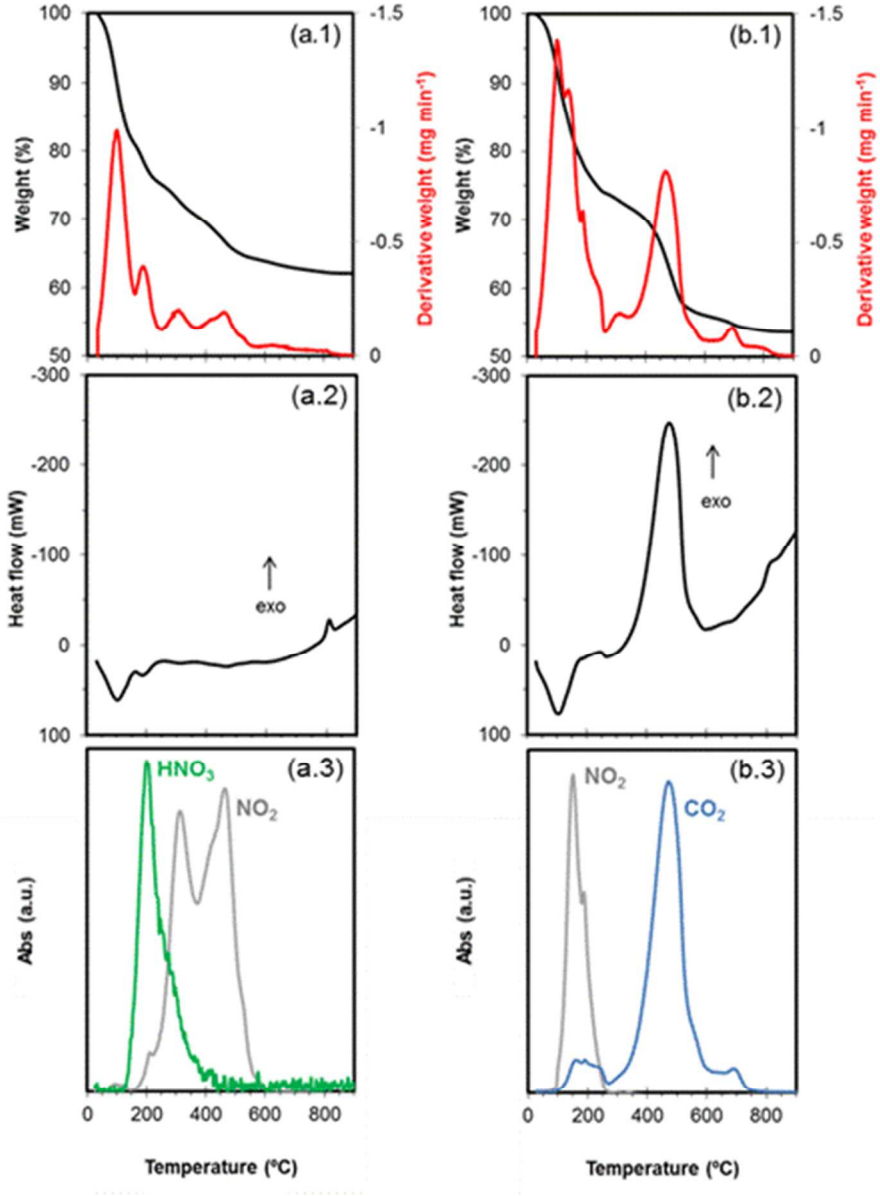

Figure 1. TGA (1) and DTA (2) analysis toghether with online gaseous FTIR spectroscopy curves (3) obtained during the thermal treatment in air atmosphere of uncalcined ZnO-I (a) and ZnO-ICP (b) samples.

The composites prepared have been investigated by XRD. Figure 2 illustrates the diffractograms obtained for the thermally treated samples from the impregnation series (ZnO-I and ZnO-ICP) and the dry mixing series (ZnO-N and ZnO-NH), along with the references of the raw materials: fresh sepiolite, sepiolite thermally treated at 500 ºC (anhydrous) and ZnO. All the diffraction peaks in the ZnO-I and ZnO-ICP patterns are readily indexed to sepiolite (anhydrous and hydrous forms) and a wurtzite structure of ZnO, indicating the complete transformation of $Zn(NO_3)_2 \cdot 6(H_2O)$ to ZnO at 500 ºC. Nevertheless, the XRD peaks are quite broad, which is due to both their low crystallinity and the small size of the crystalline domains. The X-ray diffraction patterns of the ZnO-N and ZnO-NH samples can also be indexed on the basis of a phase mixture constituted by a majority of anhydrous sepiolite and a minority of ZnO. Within the XRD resolution, there was no evidence in any sample of metallic Zn, $ZnNO_3$ or any additional phases other than sepiolite and wurtzite ZnO.

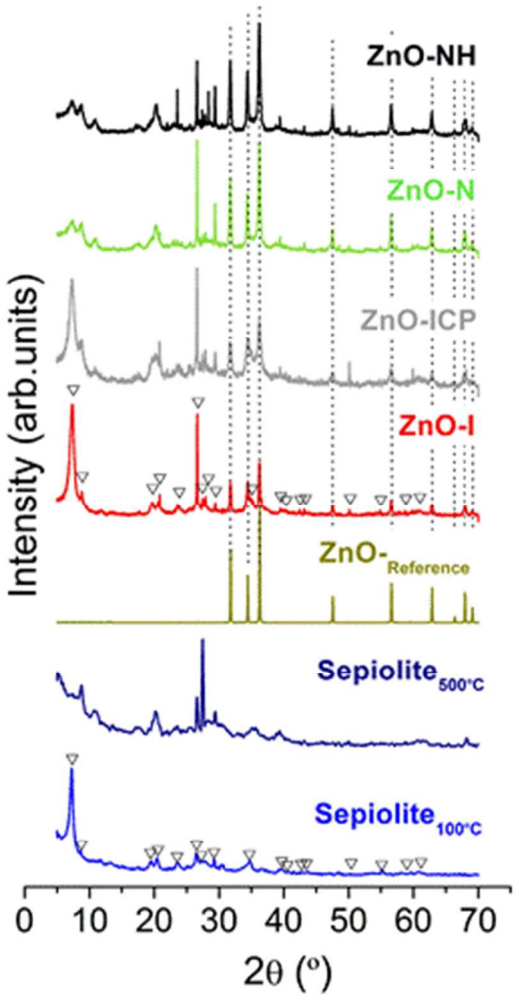

Figure 2. XRD patterns corresponding to the raw materials and the thermally treated ZnO/Sepiolite composites prepared by impregnation (ZnO-I and ZnO-ICP) and dry mixing methods (ZnO-N and ZnO-NH). The triangle symbols are associated with the sepiolite support, whereas the ZnO pattern is signaled with dash lines.

Since the samples have been calcined at 500 ºC, the coordination water of sepiolite support should have mostly been removed and the structure should have already been irreversibly folded in its anhydrous form.[31, 32] However, the diffractograms of the samples prepared by impregnation of the precursor indicate that the structure is only partially folded, because they present the characterictic reflections related to the hydrated form of sepiolite, especially the one at 2θ=7.5, in addition to those of the folded sepiolite. This effect has been confirmed by TGA-DTA analysis of the calcined ZnO-I and ZnO-ICP samples (see Supporting Information Figures S3 b and c), where the folding of the structure by loss of the coordinating water is still observed at around 260 ºC. Conversely,

the samples prepared by dry mixing with ZnO nanoparticles behave as expected and do not show any of the XRD peaks of the hydrated form. XRD analyses suggest, therefore, that the removal of water coordinated to Mg atoms of sepiolite is modified due to the interaction between the ionic species of the precursor and sepiolite, for instance redox reactions or partial ion exchange of the Mg cations by Zn^{2+}.[33].

Regarding the composition, chemical analyses by ICP-OES indicate that all the samples prepared contain 19±1 wt.% ZnO, close to the nominal 20 wt.% zinc oxide and 80 wt.% sepiolite composition. Besides the main components, the samples contained 4 wt% Al_2O_3, 20 wt% MgO, 55 wt% SiO_2 and other minor compounds from the sepiolite.

The textural characterization indicates that all samples present similar type IV N_2 adsorption/desorption isotherms, typical of materials with mesopores such as sepiolite. When ZnO nanoparticles were used in the synthesis, the nanodispersed samples exhibit a BET surface area of 112 $m^2 \cdot g^{-1}$, slightly higher than when the precursor of the salt was impregnated on the sepiolite (102 $m^2 \cdot g^{-1}$) or on the activated carbon (96 $m^2 \cdot g^{-1}$), which indicates that the smallest pores of sepiolite have been partially blocked in the impregnation procedure. ZnO-I sample exhibits a total porosity obtained by mercury intrusion of 50 %, which is slightly lower than the porosities exhibited by the samples prepared by dry mixing, both around 58%. The pore size distribution of the materials, shown in Figure 3, elucidates why the sample obtained by the impregnated carbon procedure presents the highest porosity (68%). This high porosity is related to its bimodal pore size distribution, with a maximum in the mesopore range (35 nm), like the rest of the samples, and another at 2.5 μm, associated to the macroporosity created by the elimination of the activated carbon during the calcination. A similar generation of macroporosity has been observed for other samples prepared by this method.[28]

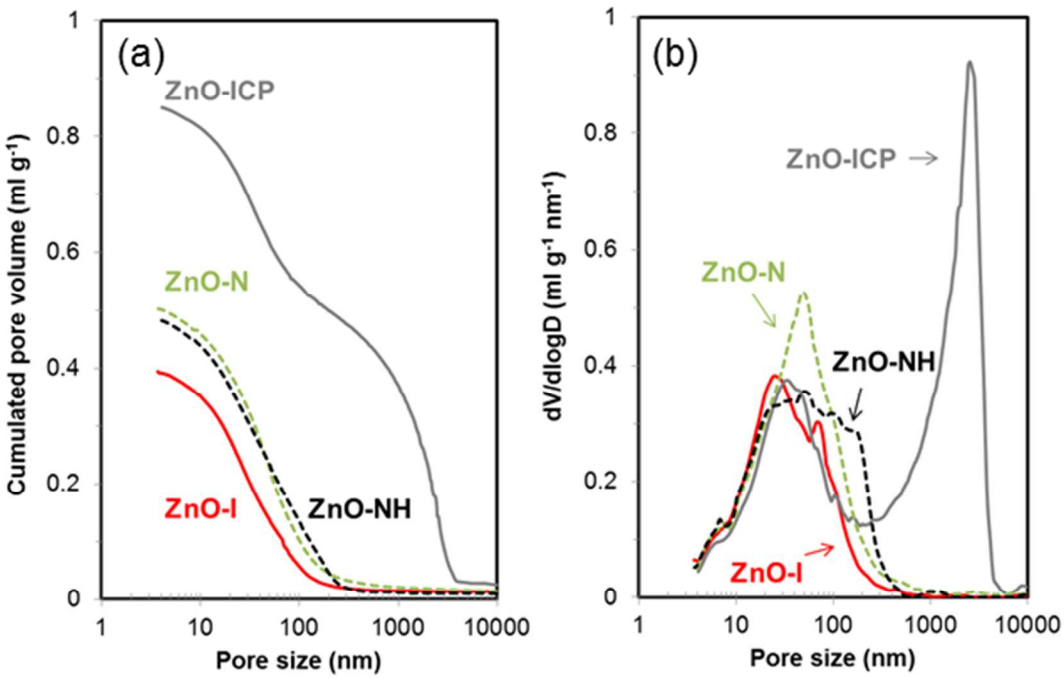

Figure 3. Cumulated pore volume (a) and pore size distribution (b) obtained by mercury intrusion porosimetry of ZnO/sepiolite composites.

In order to clarify the dispersion state of the ZnO nanoparticles supported on the sepiolite, TEM characterization has been carried out on the ZnO/sepiolite series. The micrographs, presented in Figure 4, illustrate the characteristic fibrous structure of sepiolite.[15, 18] Next to each image a scheme of the ZnO/sepiolite materials is proposed based on the TEM results, illustrating the agglomeration state and distribution of the ZnO nanoparticles on the sepiolite fibers. Figure 4(a.1) contains a HRTEM image of the ZnO/sepiolite sample prepared by impregnation showing the high agglomeration and heterogeneous distribution of the ZnO nanoparticles on the sepiolite fibers. The nanoparticles average sizes cover a broad range, between 40 and 60 nm, and agglomerates of approximately 200 nm are formed (see the scheme in Figure 4(a.2)). The lattice spacing of the nanoparticles obtained by HRTEM is ~ 1.385 Å, which is indexed as the ZnO (112) plane according to JCPDS file #79-0206. This result supports the phase assignment of the ZnO-I XRD bands of Figure 2 reported before. Figures S1(a.1-a.3) provide supporting information about the crystalline assignment of the ZnO-I composites.

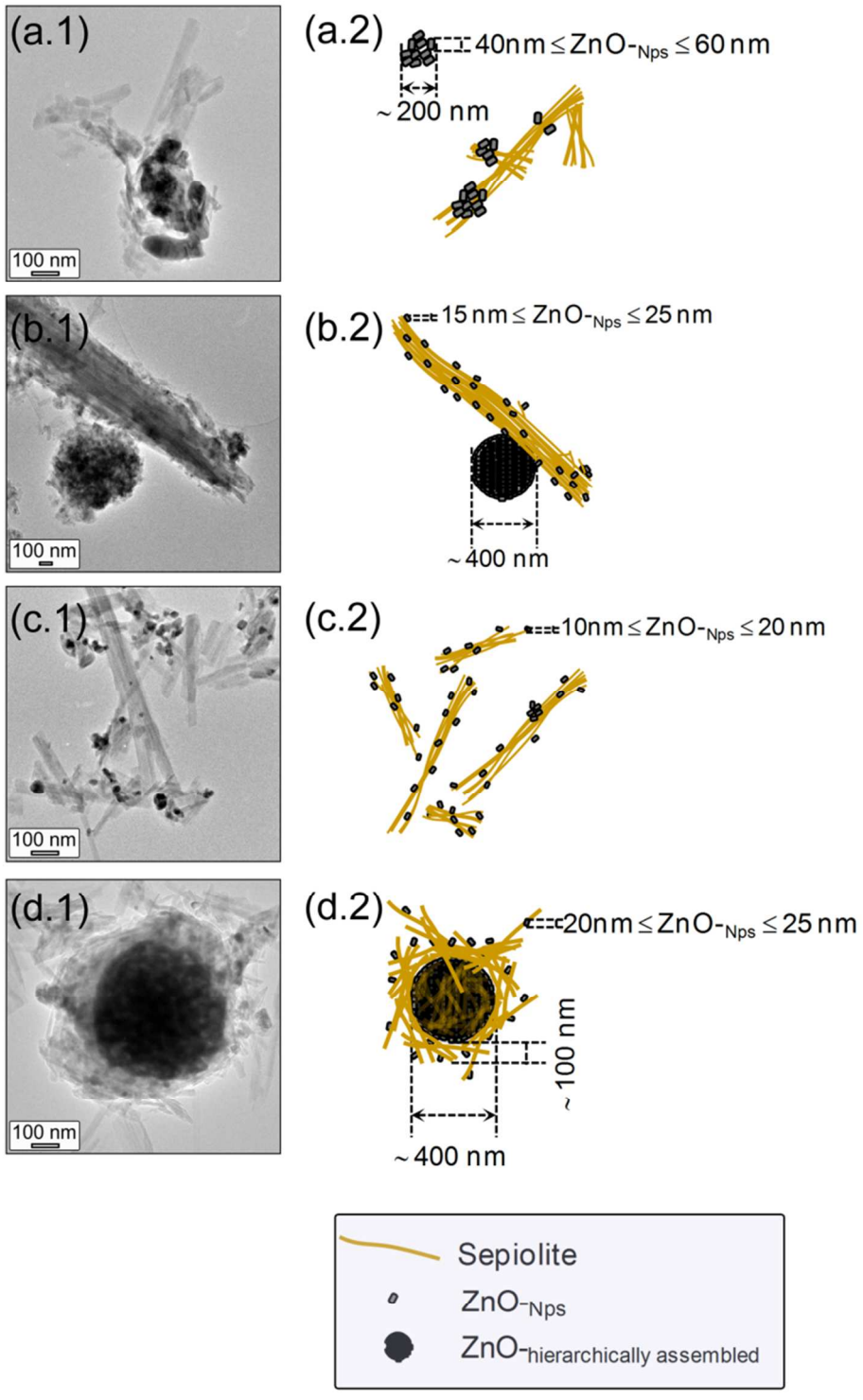

Figure 4. TEM images **(1)** and proposed cartoon **(2)** of the thermally treated samples synthesized by impregnation method, ZnO-I **(a)**, by impregnated carbon procedure, ZnO-ICP **(b),** and by dry mixing with isolated ZnO nanoparticles, ZnO-N **(c),** and hierarchically organized nanoparticles, ZnO-NH **(d)**.

The composites obtained by the impregnated carbon procedure present two different agglomeration patterns, according to Figure 4(b): disperse ZnO nanoparticles of 15-25 nm supported on sepiolite and agglomerates of ZnO nanoparticles with size around 400 nm. Again, the lattice spacing of the nanoparticles has been determined and is consistent with that of ZnO. In this case, polycrystalline domains are observed, where the lattice distances are ~ 2.462 Å (black trace), ~1.630 Å (yellow trace) and ~ 1.477 Å (red trace), which match well with that of the (101), (110) and (103) planes (JCPDS# 79-0206), respectively. See Supporting Information Figures S4(b.1-b.3).

The above experimental proofs demonstrate that the impregnation process, used in ZnO-I and ZnO-ICP series, leads to agglomeration and an uneven distribution of zinc oxide nanoparticles on the sepiolite support. They are grouped in 3D aggregates and form bulk oxide phase that lead to a poor dispersion of the active phase.

TEM also unveils details of the ZnO/sepiolite composites prepared by the dry-mixing method. Figure 4(c.1) shows a low-magnification image where the ZnO-N structure can be clearly observed. Isolated ZnO nanoparticles are highly and uniformly monodispersed on the sepiolite fibers, with 10-20 nm average size, as its cartoon depicts in Figure 4(c.2). This uniform dispersion is consistent with the narrower pore size distribution of ZnO-N. HRTEM images in Figure S4(c) show that the nanoparticles present a lattice spacing consistent with the (110) and (112) planes of ZnO phase.

Unlike the series with isolated nanoparticles, the ZnO-NH materials, dry-mixed with hierarchically organized ZnO nanoparticles, present a completely different morphology. TEM image in Figure 4(d.1) shows that, in this particular case, ZnO aggregates favor the deposition of sepiolite fibers on their surface, which is completely and uniformly covered by the clay. ZnO-NH consists of spheres of hierarchically organized nanoparticles coated by sepiolite fibers, creating a core-shell-type structure depicted in the cartoon of Figure 4(d.2). The diameter of the ZnO core is ~ 400 nm, meanwhile the thickness of the shell created by the sepiolite fibers coating is near 100 nm.

The low isoelectric point of sepiolite ($IEP_{sepiolite}$~2[34]) faccilitates the interaction with positively charged ions such as Zn^{2+}, or with compounds with high isoelectric point, which is the case of ZnO (IEP_{ZnO} ~9[35]). When powdered ZnO nanoparticles and sepiolite fibres are stirred together, the good contact and soft conditions faccilitate their mixing maintaining the original morphology: the nanodispersed particles are well dispersed on the

sepiolite fibres, meanwhile the hierarchically organized spheres, due to their size, are covered by the sepiolite, and only few nanoparticles are dispersed on the sepiolite fibres covering the agglomerates. The trend of sepiolite to cover the metal oxide particles has been previously observed as well for TiO_2,[34] Rh/Al_2O_3,[36] and VO_x-ZrO_2-SO_4^{2-}.[37] When the active phase is incorporated by impregnation, the zinc oxide formation process favors the agglomeration at the concentration of precursor employed: on the impregnated sepiolite fibers only small agglomerates form, meanwhile the preimpregnation of the activated carbon particles, in much lower amount than sepiolite (30 g of activated carbon per 100 g of final material, containing 80 wt.% sepiolite), results in the concentration of the precursor in its pores, which leads to the formation of bigger agglomerates. ZnO is formed before the carbon burnout, according to Figure S2(b), and therefore despite the affinity of sepiolite for the oxide it is only partially dispersed after the elimination of the activated carbon with generation of macroporosity. Thus, with this preparation method two agglomeration patterns appear.

In summary, ZnO-I and ZnO-ICP materials exhibit a different tendence to agglomeration and heterogeneous distribution of zinc oxide nanoparticles on the sepiolite fibers; meanwhile the main feature of the ZnO-N samples is the high dispersion of isolated zinc oxide nanoparticles on the sepiolite surface. Finally, in ZnO-NH the hierarchically organized nanoparticles of the oxide are surrounded by fibers of sepiolite. These four preparations deliver different scenarios for H_2S removal studies.

3.2. H_2S chemisorption by ZnO/sepiolite systems in inert atmosphere

Blank tests performed without any sample and with pure sepiolite showed that there is no significant H_2S elimination in the absence of ZnO. However, in the presence of the active phase H_2S is removed when adequate temperatures are reached. The activity of the different ZnO/sepiolite samples is calculated according Eq.1-3:

$$H_2S \text{ conversion} = \frac{[H_2S]_{in} - [H_2S]_{out}}{[H_2S]_{in}} \quad \text{Eq. 1}$$

$$SO_2 \text{ selectivity} = \frac{[SO_2]_{out}}{[H_2S]_{in} - [H_2S]_{out}} \quad \text{Eq. 2}$$

$$SO_2 \text{ yield} = \frac{[SO_2]_{out}}{[H_2S]_{in}} \quad \text{Eq. 3}$$

At this point it must be mentioned that the online microGC detected in the reactor inlet, besides the desired concentration of H_2S, trace amounts of carbonyl sulfide (COS), which is formed in the H_2S/N_2 cylinder. COS is completely removed at similar temperatures as H_2S in presence of the ZnO/sepiolite composites. This fact may be significant since COS, which is formed by reaction of hydrogen sulfide with carbon oxide or carbon dioxide, is a typical problem in many desulfurization applications, because it is highly corrosive [38] and presents low reactivity with ZnO.[6, 39-41] During the blank tests performed, COS was removed by sepiolite, but not by SiC, which is indicative of possible synergistic effects using sepiolite as support for ZnO. However, COS elimination is beyond the scope of this work and no further analyses on this issue will be made.

H_2S conversion and yield to SO_2 obtained with the ZnO/sepiolite composites are illustrated in Figure 5. H_2S adsorption is negligible at 50 ºC, but all samples present activity for H_2S elimination at higher temperature. It is known that hydrogen sulfide reacts with zinc oxide to form zinc sulfide according to Eq.4.

$$ZnO_{(s)} + H_2S_{(g)} \overset{\Delta Q}{\rightarrow} ZnS_{(s)} + H_2O_{(g)} \qquad \text{Eq. 4}$$

S atoms gradually replace the O atoms in the solid active phase, yielding water molecules that are desorbed to the gas phase. No other reaction products are observed in the outlet gas stream during at least 4h. However, later, at higher temperatures, when H_2S conversion values are above 50 %, SO_2 in generated in low increasing amounts. Apparently, at high temperatures and when some saturation is achieved, part of the S retained as sulfide on the surface is oxidized to SO_2, and then desorbed, in a reaction similar to the regeneration process described by Eq. 5:[5, 6, 42]

$$2ZnS_{(s)} + 3O_{2(g)} \overset{\Delta Q}{\rightarrow} 2ZnO_{(s)} + 2SO_{2(g)} \qquad \text{Eq. 5}$$

In absence of oxygen molecules, the oxidation could take place by reaction with surface hydroxyls, either coming from the sepiolite support or generated during the sulfidation process and retained in the composite.

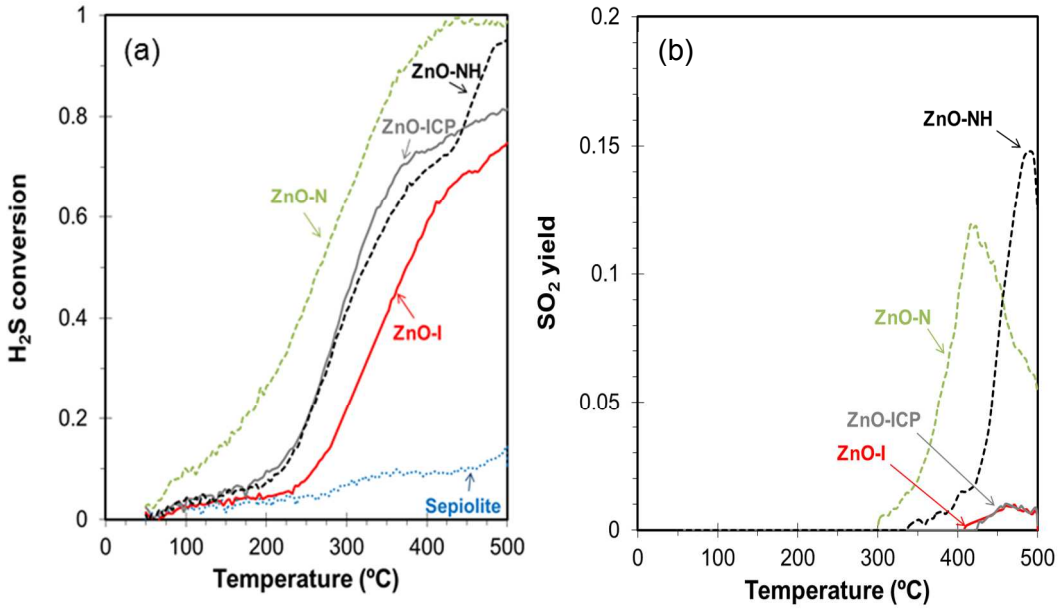

Figure 5. Temperature programmed reactive adsorption of H_2S by ZnO/sepiolite composites in inert atmosphere. Conversion as a function of the temperature (a), yield to sulfur dioxide as a function of the temperature (b).

ZnO-N, with homogeneously nanodispersed particles, is the most active material; some H_2S sorption is observed even at low temperatures and all the H_2S is retained above 400 ºC. On the contrary, ZnO-I, with the most aggregared particles, is the worst sorbent, with a maximum molar conversion of 0.75, obtained at 500 ºC. In both cases, sulfur dioxide appears in the outlet when hydrogen sulfide molar conversion values exceed 0.6, at 300 ºC for ZnO-N and 400 ºC for ZnO-I. However, the selectivity of the process to SO_2 is very low: only 1% of the pollutant removed is transformed into the oxide at 0.75 molar conversion, the rest remains stored in the active phase. The selectivity to the oxide of the nanodispersed material is higher than 5% only above 0.9 molar conversion.

ZnO-NH and ZnO-ICP samples possess similar morphology (some dispersed particles of about 20 nm and agglomerates of 400 nm) and both exhibit similar performance up to 300ºC, where they remove 45% of the pollutant. This is somewhere between the performance of dispersed and aggregated systems (ZnO-N and ZnO-I). Some differences are apparent at higher temperatures: H_2S conversion with ZnO-NH sharply increases, accompanied by a higher selectivity to SO_2. This effect has not been observed in the other samples and could be related to the significantly different ZnO/sepiolite dispersion of ZnO-NH composite. The core-shell-type structure, with sepiolite covering the ZnO core, seems to present a good contact between the oxidizing species and the sulfided core and not to

affect the accessibility of H_2S to the ZnO particles. Regarding the ZnO-ICP composite, its characteristics favor H_2S conversion with respect to the ZnO-I sample, which might be a consequence of the higher porosity achieved with the elimination of the activated carbon, but with a similar trend and similar low yield to SO_2. The sulphurous oxide is not detected until a 0.75 H_2S molar conversion is attained, at 400ºC.

3.3. Comparison of H_2S chemisorption in inert atmosphere and in the presence of O_2

In order to compare and understand the reaction mechanism, the most active sample (ZnO-N) was also tested for hydrogen sulfide removal from an air stream in the same operating conditions. Figure 6 shows the temperature programmed evolution of the reactor outlet composition over time in the presence and absence of oxygen.

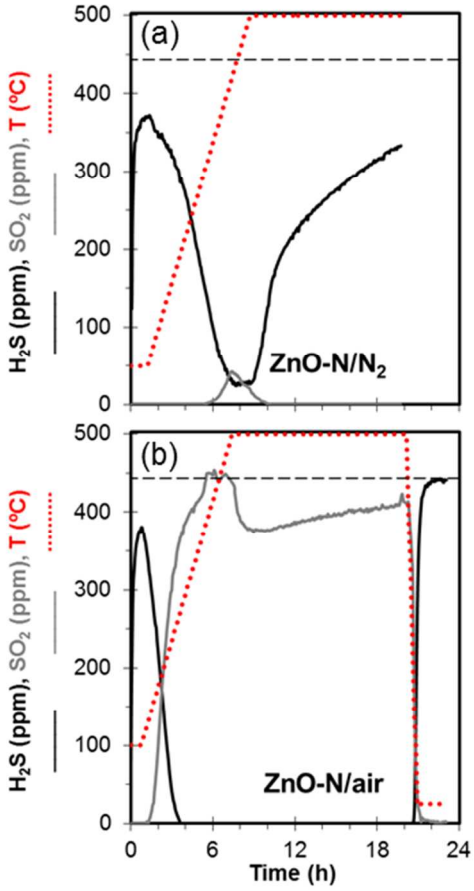

Figure 6. Temperature programmed H_2S removal by ZnO-N sample in inert atmosphere (a) and in the presence of O_2 (b).

The different performance of ZnO-N composite with hydrogen sulfide in both environments is dramatic. In the absence of oxygen, the reaction demands higher temperatures to occur, and the conversion decreases as the available active site become fewer due to the replacement of available oxide ions by sulfide ions. In air, however, total H_2S chemisorption is achieved below 300 ºC and hydrogen sulfide is almost completely oxidized to sulfur dioxide above ca. 400 ºC. Furthermore, no deactivation of the sample is observed after 17 h operation with total conversion (the last 13 h at 500 ºC). The sorbent acts as a catalyst, since the sulfided ZnO is constantly regenerated, yielding SO_2. An additional test was performed in air with just pure sepiolite, without ZnO. Hardly any SO_2 is generated, although some H_2S removal is observed while heating from 100 to 500 ºC, but H_2S removal quickly decayed to virtually zero upon reaching and holding 500 ºC. This result indicates that in the operating conditions studied the noncatalytic combustion of H_2S to give SO_2 is limited, confirming that the combustion observed in the presence of the ZnO/sepiolite composite is catalytic.

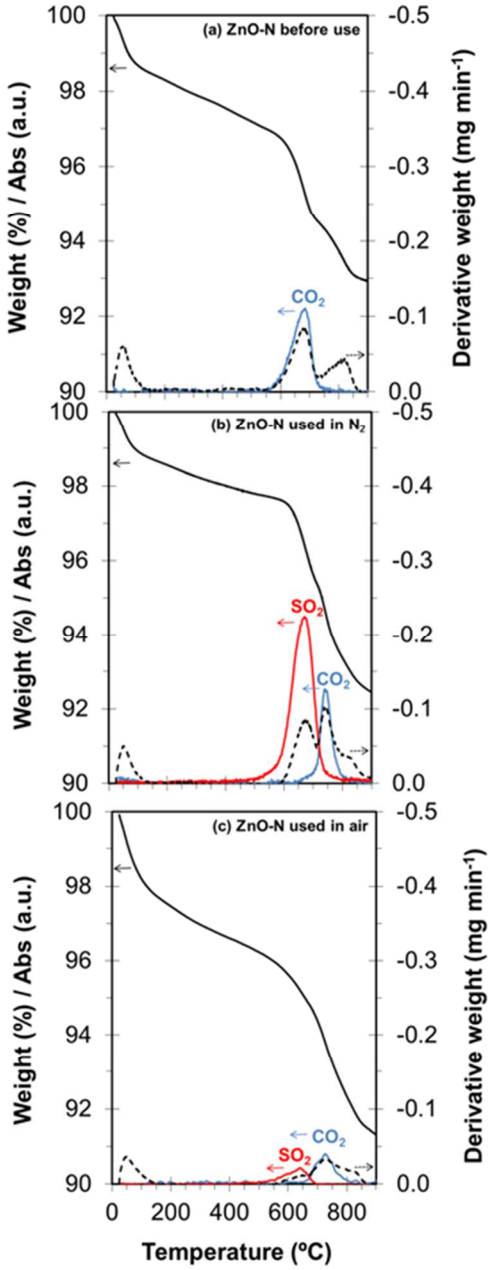

Figure 7. Thermal analysis in flowing air of ZnO-N sample: fresh (a), and after use for H_2S elimination in inert atmosphere (b), or in the presence of O_2 (c).

Figure 7 shows the results obtained in the TGA-DTA-FTIR analysis of ZnO-N as-calcined and after use in both environments. As it has been commented above, after the calcination of these samples the sepiolite structure is already irreversibly folded in the anhydrous form because most of the coordination water of has been removed, and consequently only the reversible elimination of the hygroscopic water is observed. Besides other two transformations related to the support are produced. The first weight loss takes place at

approximately 678 ºC, with simultaneous CO_2 formation. This weight loss must be related to the decomposition of the carbonate impurities of the sepiolite, such as calcite.[43] The second weight loss takes place at 820 ºC and is related to the exothermal sepiolite-to-enstatite transformation, with loss of the structural water by dehydroxylation acording to Eq. 6:[44, 45]

$$Mg_8Si_{12}O_{30}(OH)_4 \rightarrow 8MgSiO_3 + 4SiO_2 + 2H_2O \qquad \text{Eq. 6}$$

These phenomena are observed in Figure 7 a, b and c, but at higher temperatures in the samples used for hydrogen sulfide chemisorption, especially the first transformation that is retarded to 744 ºC. Additionally a new endothermic weight loss occurs at lower temperature, with a maximum at 670 ºC. This weight loss is produced by the reaction of oxygen with the sulfided surface to regenerate the zinc oxide yielding gaseous SO_2, as the online IR gas cell indicates. The amount of SO_2 released from the sample used for H_2S elimination in oxidizing atmosphere is very low because most of the H_2S removed in the presence of O_2 is converted to SO_2 and released to the atmosphere, preventing the deactivation of the catalyst. In inert atmosphere it is kinetically difficult for a sulfur atom to remove several oxygen atoms from ZnO to form a sulfur oxide.[46] Thus, instead, sulfide ions easily replace oxide ions in ZnO lattice, which possesses the same structure as ZnS, and this accumulates sulfur. Consequently, a significantly higher amount of SO_2 forms during the thermal analysis of the sample used in N_2. These profiles show that the elimination of sulfur starts at 500 ºC and is complete below 750 ºC. Similar regeneration temperatures have been reported in the literature for Zn-based sorbents.[4, 5] The absence of weight gain during the thermal treatment in O_2-containing atmosphere cannot discard the formation of intermediate oxidized sulfur species at lower temperature before total desulfurization takes place[40, 42, 47], because this effect may be masked by the weight loss.

The TGA-FTIR results for ZnO-N are consistent with the XRD patterns of the used ZnO-N samples depicted in Figure 8. The X-ray diffraction patterns of the fresh and used ZnO-N (Figure 2 *versus* Figure 8) indicate that its crystalline structure did not change upon use for H_2S elimination in air: the diffraction peaks of sepiolite and ZnO present similar relative intensities. However, the crystalline structure is modified upon use for H_2S chemisorption in N_2 flow: the partial substitution of its oxide ions by sulfide ions is illustrated by the development of the diffraction peaks of ZnS and the weakeing of the intensity of the ZnO peaks.[5]

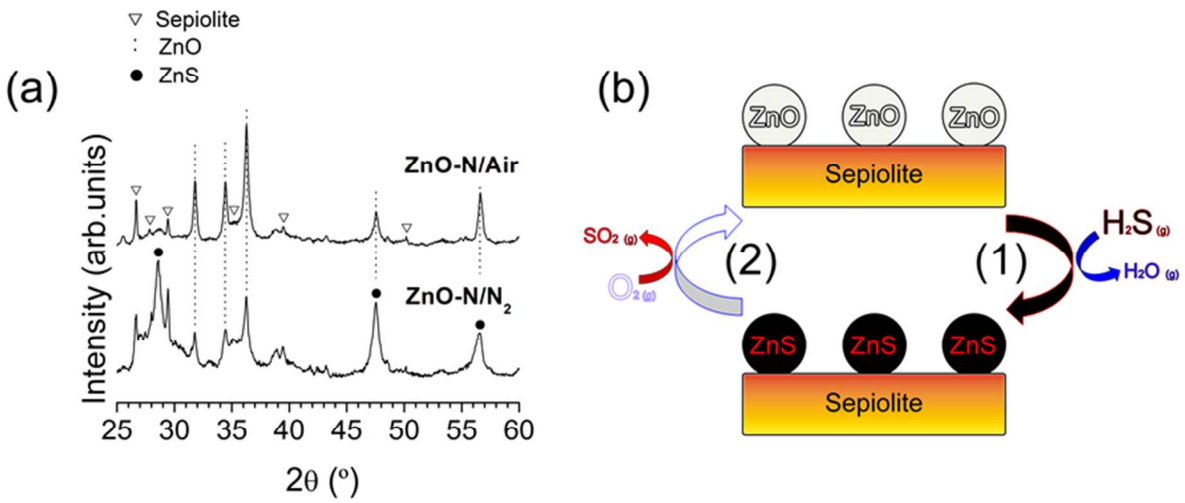

Figure 8. (a) XRD patterns of ZnO-N sample: after use for H_2S elimination in inert atmosphere (N_2), or in the presence of O_2 (air). **(b)** Schematic representation of H_2S chemisorption mechanism on the ZnO-N system, which is characterized by two steps: **(1)** Hydrogen sulfide reacts with zinc oxide to form zinc sulfide, and **(2)** ZnO is regenerated by reaction of ZnS with O_2.

The data presented above suggest that H_2S removal takes place in two steps, illustrated in Figure 8(b), which depend on the reaction conditions. The cartoon was developed based on TGA-FTIR and XRD information to describe the observed trends. Step (1) consists in the reaction of the ZnO nanoparticles with hydrogen sulfide to produce zinc sulfide (Eq. 3) and can take place under both reaction conditions, in an inert atmosphere, such as N_2, as well as in presence of O_2 (oxidizing reaction conditions). The sulfidation of ZnO is reversible under oxidizing conditions (Eq. 4), which is represented by the reaction process marked as (2) in Figure 8(b). Therefore, in air atmosphere both processes (1) and (2) occur, the latter at a faster rate, and the activity for H_2S-to-SO_2 conversion is maintained over time. Conversely, in an inert atmosphere only the first step may take place and oxide ions are progresively replaced.

3.4. Isothermal H_2S removal

In order to proof that the activity of the spent ZnO/sepiolite system may be regenerated by thermal treatment in presence of O_2 and to evaluate the sulfur capacity of the sorbent the isothermal experiment depicted in Figure 9 was performed with the ZnO-N sample at 500 ºC in a 1L min^{-1} gas flow with variable composition. In a first step H_2S was fed in oxidating conditions and it was totally removed and converted into SO_2; when H_2S was removed from the feed no more S-compunds were detected in the outlet. Then the system was

purged with N_2, and H_2S was added again to the feed in by-pass before switching to the reactor to evaluate the sorption capacity in inert conditions. The accumulated sorption capacity in inert atmosphere of this material at 500 ºC was measured to be 140 mg S/g ZnO before H_2S concentration in the outlet reaches 10 ppm. After 9 h operation, H_2S in the outlet was 246 ppm and the sulfur capacity reached 336 mg S/g ZnO, 86 % of the theoretical sulfur capacity if all the ZnO is consumed (393 mg S/g ZnO). The saturation capacity estimated from the length of unused bed (LUB), calculated with the breakthrough (0.1) and stoichiometric points (3.6 and 6.9 h, respectively), is 350 mg S/g ZnO, 89% of the theoretical value. The long time needed to saturate the adsorbent is associated to mass transfer limitations because the reaction system has not been optimized. Smaller pellets would reduce the void volume and improve the diffusion phenomena.

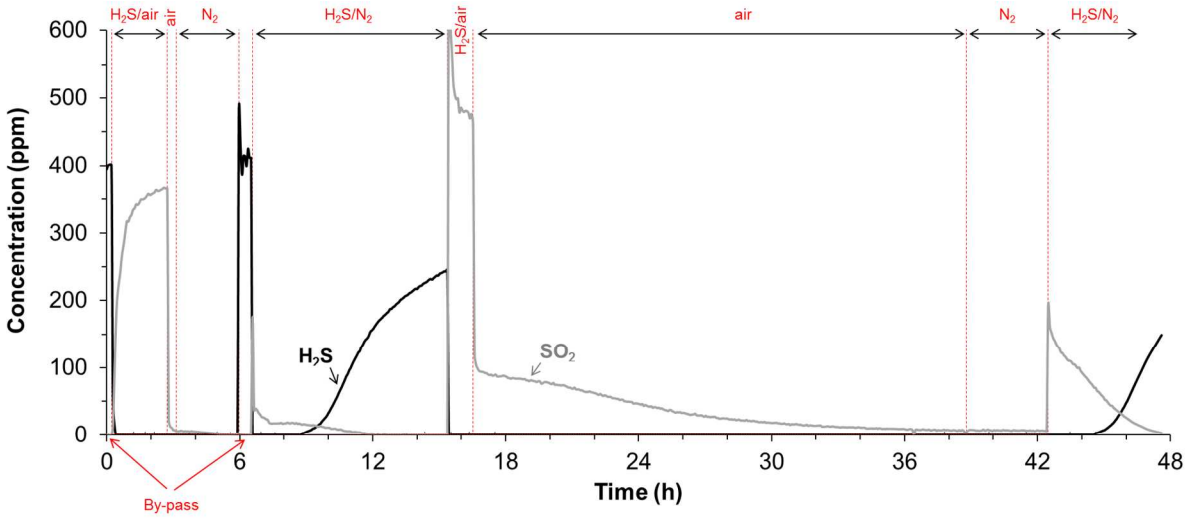

Figure 9. Performance of ZnO-N sample in a continuous experiment including H_2S removal in the presence of O_2, H_2S removal in inert atmosphere until deactivation, regeneration, and subsequent H_2S removal in inert atmosphere. Temperature = 500 ºC.

Almost identical H_2S sorption capacity was obtained in a second use under inert atmosphere after regeneration in air, indicating that the ZnO was recovered and the lean temperature employed did not substantially affect the properties of the ZnO/sepiolite composite. However, the regeneration time was long and a fraction of the oxidized sulfur species formed under air flow remained initially adsorbed on the surface, probably as $ZnSO_3$, since the S atom of the formed SO_2 bonds to a surface oxygen atom to from an analogical SO_3 structure[48]. In inert atmosphere and once hydrogen sulfide is added these species are decomposed and SO_2 desorbs until their total consumption. As Figure 7 indicates, higher regeneration temperatures would facilitate a complete and faster removal

of the sulfur species from the spent sorbent. However, processes such as sintering or volatilization of the active phase[10] or porosity shrinkage must be carefully controlled. ZnO regeneration is still subject of optimization and has been investigated by several authors[10, 48], because on one side the sorbent can be reactivated, and on the other side the SO_2 obtained can be valorized to avoid its accumulation as pollutant. Sulfur dioxide can be used to produce H_2SO_4, one of the chemicals manufactured in largest quantity in terms of mass, or as preservative in the food industry (labeled as E220 in Europe), for instance for wine and dried fruits.

4. Conclusions

Sepiolite can be used as binder and support to obtain monoliths with nanostructured ZnO by the four preparation methods explored, two based on impregnation with a soluble zinc precursor and two based on dry mixing with ZnO nanoparticles. The properties of the composites depend on the preparation method. The removal of coordinated water to obtain the anhydrous form of sepiolite is partially hindered by the interaction/reaction of sepiolite with the precursor ions, more precisely with Zn^{2+}, since many metallic nitrates have been previously used as precursors to synthetize sepiolite-supported catalysts and this effect was not observed. The impregnated active carbon procedure demands calcination temperatures above 500 ºC to ensure thorough carbon combustion, whereby macroporosity is generated. The activity results are consistent with an H_2S removal cycle occurring in two stages: (1) Hydrogen sulfide reacts with zinc oxide to form zinc sulfide and water is generated; this process takes place in both an inert atmosphere and in the presence of O_2. (2) Reoxidation of the sulfided surface with generation of sulfur dioxide; this step is only possible under oxidizing conditions, and does not happen in inert atmospheres, where the sulfur is accumulated as ZnS. The activity for H_2S sorption is favoured in the composites prepared by dry mixing of the clay with dispersed ZnO nanoparticles, where the nanostructure of the ZnO used is maintained. The use of ZnO nanoparticles adds green chemistry[49] and economical value to the synthesis of a material for environmental remediation, since zinc salts precursors need impregnation, drying and calcination steps. In order to recover the activity the spent material must be heated in an oxidizing atmosphere. The presence of water could further improve the performance of the materials.[39, 50]

Finally, it should be emphasized that the general strategy and design principles described in this study open the possibility of obtaining ZnO/sepiolite composites conformed as honeycomb monoliths to minimize the emission of pollutants such as hydrogen sulfide.

5. Acknowledgements

The authors would like to express their thanks for financial support to MINECO (Spain) for the projects MAT2013-48009-C4-1-P and CTQ2011-25517-PPQ and the *Juan de la Cierva* contract of Dr. R. Portela (JCI-2010-08221). Dr. F. Rubio-Marcos is also indebted to CSIC for a *Junta de Ampliación de Estudios* contract (JAEDOC071), which is co-financed with FEDER funds.

6. References

1. S. Yaşyerli, İ. Ar, G. Doğu and T. Doğu, *Chem. Eng. Process.*, 2002, 41, 785-792.
2. T. J. Bandosz, *Catal. Today*, 2012, 186, 20-28.
3. D. Nguyen-Thanh, K. Block and T. J. Bandosz, *Chemosphere*, 2005, 59, 343-353.
4. M. Xue, R. Chitrakar, K. Sakane and K. Ooi, *Green Chem.*, 2003, 5, 529-534.
5. H. F. Garces, H. M. Galindo, L. J. Garces, J. Hunt, A. Morey and S. L. Suib, *Microporous Mesoporous Mater.*, 2010, 127, 190-197.
6. A. Samokhvalov and B. J. Tatarchuk, *Phys. Chem. Chem. Phys.*, 2011, 13, 3197-3209.
7. A. L. Kohl and R. Nielsen, *Gas Purification*, Elsevier Science, 1997.
8. T. Baird, K. C. Campbell, P. J. Holliman, R. Hoyle, D. Stirling and B. P. Williams, *J. Chem. Soc., Faraday Trans.*, 1995, 91, 3219-3230.
9. E. García, C. Cilleruelo, J. V. Ibarra, M. Pineda and J. M. Palacios, *Ind. Eng. Chem. Res.*, 1997, 36, 846-853.
10. X. M. Meng, W. De Jong and A. H. M. Verkooijen, *Environ. Prog. Sustain. Energy*, 2009, 28, 360-371.
11. P. Dhage, A. Samokhvalov, D. Repala, E. C. Duin and B. J. Tatarchuk, *Phys. Chem. Chem. Phys.*, 2011, 13, 2179-2187.
12. M. Tsukada, K. Abe, Y. Yonemochi, A. Ameyama, H. Kamiya, S. Kambara, H. Moritomi and T. Uehara, *Powder Technol.*, 2008, 180, 232-238.
13. I. V. Babich and J. A. Moulijn, *Fuel*, 2003, 82, 607-631.
14. W. G. Xu, S. F. Liu, S. X. Lu, S. Y. Kang, Y. Zhou and H. F. Zhang, *J. Colloid Interface Sci.*, 2010, 351, 210-216.
15. A. Álvarez, in *Palygorskite-sepiolite occurrences, genesis, and uses* eds. A. Singer and E. Galán, Elsevier, Amsterdam, 1984, vol. 37, pp. 253-289.
16. A. Álvarez, J. Santarén, A. Esteban-Cubillo and P. Aparicio, in *Developments in Clay Science*, eds. G. Emilio and S. Arieh, Elsevier, 2011, vol. Volume 3, pp. 281-298.
17. P. Avila, M. Montes and E. E. Miro, *Chem. Eng. J.*, 2005, 109, 11-36.

18. S. Suárez, J. M. Coronado, R. Portela, J. C. Martín, M. Yates, P. Ávila and B. Sánchez, *Environ. Sci. Technol.*, 2008, 42, 5892-5896.
19. R. Portela, R. F. Tessinari, S. Suarez, S. B. Rasmussen, M. D. Hernandez-Alonso, M. C. Canela, P. Avila and B. Sanchez, *Environ. Sci. Technol.*, 2012, 46, 5040-5048.
20. S. B. Rasmussen, R. Portela, S. Suárez, J. M. Coronado, M. L. Rojas-Cervantes, P. Avila and B. Sánchez, *Ind. Eng. Chem. Res.*, 2010, 49, 6685–6690.
21. L. Daza, S. Mendioroz and J. A. Pajares, *Clays Clay Miner.*, 1991, 39, 14-21.
22. M. I. Guijarro, S. Mendioroz and V. Muñoz, *Appl. Catal., A*, 1995, 132, 335-351.
23. R. Schlögl, M. Che, O. Clause, C. Marcilly, C. Louis, H. Knöinger, E. Teglauer, W. Keim, B. Drieben-Hölscher, J. W. Geus, A. J. van Dillen and J. Barbier, in *Handbook of Heterogeneous Catalysis*, Wiley-VCH Verlag GmbH, 2008, DOI: 10.1002/9783527619474.ch2b, pp. 138-264.
24. A. Van Dillen, R. Terorde, D. Lensveld, J. Geus and K. Debjong, *J. Catal.*, 2003, 216, 257-264.
25. N. Job, M. F. R. Pereira, S. Lambert, A. Cabiac, G. Delahay, J.-F. Colomer, J. Marien, J. L. Figueiredo and J.-P. Pirard, *J. Catal.*, 2006, 240, 160-171.
26. F. Rubio-Marcos, V. Calvino-Casilda, M. A. Bañares and J. F. Fernandez, *J. Catal.*, 2010, 275, 288-293.
27. F. Rubio-Marcos, E. Rojas, R. López-Medina, M. O. Guerrero-Pérez, M. A. Bañares and J. F. Fernandez, *ChemCatChem*, 2011, 3, 1637-1645.
28. J. Blanco, A. L. Petre, M. Yates, M. P. Martin, J. A. Martin and M. A. Martin-Luengo, *Appl. Catal., B*, 2007, 73, 128-134.
29. J. Shi, Y. Liu, Q. Peng and Y. Li, *Nano Res.*, 2013, 6, 441-448.
30. F. Rubio-Marcos, V. Calvino-Casilda, M. A. Bañares and J. F. Fernandez, *ChemCatChem*, 2013, 5, 1431-1440.
31. R. L. Frost and Z. Ding, *Thermochim. Acta*, 2003, 397, 119-128.
32. H. Nagata, S. Shimoda and T. Sudo, *Clays Clay Miner.*, 1974, 22, 285-293.
33. A. Esteban-Cubillo, R. Pina-Zapardiel, J. S. Moya, M. F. Barba and C. Pecharromán, *J. Eur. Ceram. Soc.*, 2008, 28, 1763-1768.
34. C. Knapp, F. J. Gil-Llambias, M. Gulppi-Cabra, P. Avila and J. Blanco, *J. Mater. Chem.*, 1997, 7, 1641-1645.
35. M. Kosmulski, *Adv. Colloid Interface Sci.*, 2009, 152, 14-25.
36. S. Suárez, C. Saiz, M. Yates, J. A. Martin, P. Avila and J. Blanco, *Appl. Catal., B*, 2005, 55, 57-64.
37. S. B. Rasmussen, J. Due-Hansen, M. Villarroel, F. J. Gil-Llambias, R. Fehrmann and P. Ávila, *Catal. Today*, 2011, 172, 73-77.
38. T. E. Graedel, G. W. Kammlott and J. P. Franey, *Science*, 1981, 212, 663-665.
39. L. Li and D. L. King, *Catal. Today*, 2006, 116, 537-541.
40. R. V. Siriwardane and S. Woodruff, *Ind. Eng. Chem. Res.*, 1995, 34, 699-702.
41. E. Sasaoka, K. Taniguchi, M. A. Uddin, S. Hirano, S. Kasaoka and Y. Sakata, *Ind. Eng. Chem. Res.*, 1996, 35, 2389-2394.
42. J. M. Sánchez-Hervás, J. Otero and E. Ruiz, *Chem. Eng. Sci.*, 2005, 60, 2977-2989.
43. R. Ruiz, J. C. del Moral, C. Pesquera, I. Benito and F. González, *Thermochim. Acta*, 1996, 279, 103-110.
44. P. Avila, J. Blanco, C. Knapp and M. Yates, in *Stud. Surf. Sci. Catal.*, 1998, vol. 116, pp. 233-242.
45. V. G. Milt, E. D. Banús, E. E. Miró, M. Yates, J. C. Martín, S. B. Rasmussen and P. Ávila, *Chem. Eng. J.*, 2010, 157, 530-538.

46. S. Chaturvedi, J. A. Rodriguez, T. Jirsak and J. Hrbek, *J. Phys. Chem. B*, 1998, 102, 7033-7043.
47. H. F. Garces, A. E. Espinal and S. L. Suib, *J. Phys. Chem. C*, 2012, 116, 8465-8474.
48. L. Ling, P. Han, B. Wang and R. Zhang, *Fuel Process. Technol.*, 2013, 109, 49-56.
49. P. T. Anastas and J. C. Warner, *Green Chemistry: Theory and Practice*, Oxford University Press, New York, 1998.
50. J. M. Davidson and K. Sohail, *Ind. Eng. Chem. Res.*, 1995, 34, 3675-3677.